gels

MDPI

Article

Microscopic Depolymerization Mechanism Based on Free-Radical Degradation and Its Application in Gel Plug Removal After Polymer Flooding

Yuchen Wen [1,*], Jincai Wang [1], Yinuo Pan [2], Yincheng Liu [1], Nu Lu [1], Ruicheng Ma [1] and Jirui Hou [3,*]

[1] PetroChina Research Institute of Petroleum Exploration and Development, Beijing 100083, China
[2] Oil & Gas Technology Research Institute, PetroChina Huabei Oilfield Company, Renqiu 062550, China
[3] College of Petroleum Engineering, China University of Petroleum (Beijing), Beijing 102249, China
* Correspondence: wenyc2024@petrochina.com.cn (Y.W.); houjirui@126.com (J.H.)

Abstract

Gel plugging in wellbores and near-wellbore regions caused by polymer adsorption and retention severely hinders fluid injection and production efficiency in post-polymer flooding reservoirs. To address this issue, a highly efficient chemical plug removal agent was formulated and selected. Under reservoir conditions of 65 °C and a salinity of 6864 mg/L, the system exhibited excellent dispersion stability, with a Zeta potential of −36.7 mV. It achieved a viscosity-reduction rate exceeding 95% for polymers across various molecular weights. The microscopic degradation mechanism was elucidated based on the published literature and experimental results. Fe^{2+} activation triggered the generation of highly reactive $SO_4\bullet^-$ and HO• radicals. Under acidic conditions (pH ≤ 6), the reaction was dominated by controlled $SO_4\bullet^-$ radicals, breaking down dense three-dimensional gel networks, which dramatically reduced the aggregate size from 500~2000 nm to 10~30 nm. Dynamic coreflooding tests demonstrated that injecting the system lowered the residual resistance factor from 6.5 to 1.0~1.5, achieving a permeability recovery rate exceeding 80%. Field trial results further verified that application of the composite plug removal agent and subsequent acid stimulation decreased injection pressure from 12.5 MPa to 5.5 MPa, increasing the apparent water-injectivity index to 2.4 times its initial value. This study provides crucial theoretical insights and technical support for efficient near-wellbore unplugging and residual oil mobilization in post-polymer flooding reservoirs.

Keywords: chemical flooding; polymer degradation agent; gel plug removal; enhanced oil recovery

Academic Editor: Esmaiel Jabbari

Received: 24 September 2026
Revised: 18 October 2026
Accepted: 23 October 2026
Published: 25 October 2026

Copyright: © 2026 by the authors. Licensee MDPI, Basel, Switzerland. This article is an open access article distributed under the terms and conditions of the Creative Commons Attribution (CC BY) license.

1. Introduction

Polymer flooding is one of the most established chemical enhanced-oil-recovery (EOR) technologies for mature reservoirs. By increasing the viscosity of the injected aqueous phase, a polymer solution lowers the water–oil mobility ratio, suppresses viscous fingering, and improves areal and vertical sweep efficiency. Partially hydrolyzed polyacrylamide (HPAM) remains the dominant field polymer because it provides high viscosifying efficiency at relatively low concentrations and can be tailored over a broad range of molecular weights and degrees of hydrolysis [1–3]. Laboratory studies, pilot tests, and commercial projects have demonstrated substantial incremental recovery in both conventional and heavy-oil reservoirs [4–7].

Field performance nevertheless depends on preserving polymer viscosity and injectivity during preparation, surface handling, and transport through the reservoir. HPAM can undergo mechanical scission, hydrolysis, and oxidative degradation. Its stability is strongly affected by temperature, dissolved oxygen, transition-metal ions, pH, salinity, and hardness [2,8–10]. These effects become particularly important in mature polymer-flooded reservoirs, where repeated exposure to formation brine and long residence times may change polymer conformation, molecular weight, and solution rheology.

A further limitation is polymer retention in porous media. Adsorption on mineral surfaces, mechanical entrapment at constricted pore throats, and hydrodynamic retention can delay polymer propagation and reduce the effective pore volume [11,12]. Continued injection may therefore decrease permeability and increase the resistance and residual resistance factors. Micromodel and coreflooding studies have shown that high-molecular-weight polymers can bridge pore throats, accumulate near the inlet, and form persistent flow barriers [11,13–15]. Near-wellbore shear and extensional flow may further aggravate injectivity loss, especially when polymer molecular size and concentration are poorly matched to pore structure [16].

The gel plug in the near-wellbore region is difficult to remove because the retained material is commonly a composite of entangled polymers, crude oil, suspended solids, and inorganic deposits [17]. Water injection alone is usually insufficient to restore permeability. Mechanical stimulation has a limited treatment radius and may damage completion, whereas strong mineral acids can corrode tubing, react with the rock matrix, and generate secondary precipitates. Oxidative treatments can depolymerize retained HPAM, but uncontrolled reactions may be too rapid near the wellbore, consume the active agent prematurely, or introduce safety and corrosion risks. Combining profile control with gel plug removal can improve placement in heterogeneous media, but treatment selectivity and reaction control remain central challenges [18].

Controlled chemical depolymerization provides a mechanistically attractive route for removing polymer-related damage. Polyacrylamide can be degraded by thermal, mechanical, photolytic, biological, and oxidative pathways; among these, radical oxidation directly cleaves the carbon backbone and rapidly decreases molecular weight and viscosity [19]. Peroxydisulfate is a comparatively stable oxidant in ambient conditions, but heat or catalytic activation cleaves its peroxide bond and generates sulfate radicals ($SO_4^{\bullet-}$), which can also produce hydroxyl radicals ($HO^{\bullet}$) in water [20–23]. These reactive species attack organic macromolecules through electron transfer, hydrogen abstraction, and addition reactions, initiating chain oxidation and scission.

Persulfate chemistry is especially relevant to oilfield polymer removal because its activation rate can be regulated by temperature, pH, and transition-metal species [24]. Alkali-activated persulfate has been shown to degrade high-molecular-weight polyacrylamide and remove polymer filter cake [25]. Synergistic activation by heat and Fe(II) complexes can accelerate HPAM degradation while maintaining activity under alkaline conditions [26]. Free-radical studies further show that chain cleavage of high-molecular-weight polyacrylamide is accompanied by a pronounced decrease in molecular size and solution viscosity [27]. These findings support the use of a deliberately activated persulfate system, but the relationship among radical speciation, polymer-network disintegration, porous-medium permeability recovery, and field injectivity has not been fully established for post-polymer-flooding reservoirs.

An effective treatment must also address the multicomponent nature of plugging deposits. The oxidant should cleave the polymer backbone; a mild acid should dissolve acid-soluble inorganic material without attacking the sandstone framework or tubular steel excessively; and an oil-washing agent should mobilize crude oil and expose the

polymer-rich deposit to the reactive solution. At the same time, the formulation should remain dispersed under reservoir salinity and temperature, penetrate beyond the immediate wellbore, and avoid uncontrolled radical generation [28].

Accordingly, a persulfate-based composite plugging removal agent for gel plug removal after polymer flooding was designed in this study. The primary oxidant, activator, acid, and oil-washing agent were screened and selected. Electron paramagnetic resonance was used to identify the reactive radicals and quantify their dependence on pH and Fe2+ concentration. Changes in polymer viscosity, gel mass, particle-size distribution, and microstructure were then linked to radical-induced chain scission. Finally, long-core flooding experiments and a field trial were conducted to evaluate permeability recovery, residual resistance reduction, pressure response, and injectivity improvement. In this study, the pH-dependent speciation evolution of sulfate and hydroxyl radicals in the persulfate-Fe^{2+} system under acidic conditions is revealed, and the correlation between radical species distribution and polymer removal performance is established. The microscopic gel network destruction is linked with core-scale permeability recovery and field-scale injectivity improvement. Finally, an integrated remediation strategy targeting organic–inorganic composite near-wellbore plugging (polymer flocs, crude oil, and carbonate scaling) is proposed, instead of only treating pure polymer plugging.

2. Results and Discussion

2.1. Selection of Persulfate-Based Composite Plugging Removal Agent Formulation

2.1.1. Component Screening and Concentration Selection

(1) Screening and selection of the primary agent

Different gel plug removal agents, including oxidative, acidizing, and enzyme-based agents, were added at 0.5 wt% to a polymer solution with an initial viscosity of 748 mPa·s at 65 °C and pH 7 (Figure 1a). Benzoyl peroxide and α-amylase reduced the viscosity by less than 80%, whereas all the inorganic oxidants achieved reductions greater than 95%. Hydrogen peroxide, potassium ferrate, and sodium persulfate performed best, each exceeding 98%. Oxidants and acids are widely used but may corrode tubing, and acids may also attack the sandstone framework. Enzymes have limited temperature and salinity tolerance and react more slowly and less effectively than chemical agents. Sodium persulfate was therefore selected as the primary agent. It is nearly inert at low temperature without a catalyst but reacts rapidly with polymers at elevated temperature after activation, cleaving the backbone, shortening carbon chains, disrupting the three-dimensional network, and lowering viscosity [18,23,24].

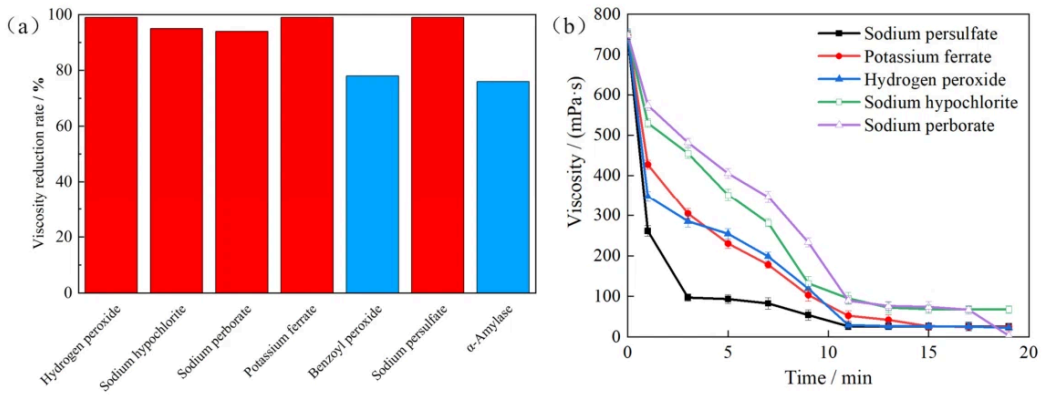


Figure 1. (**a**) Viscosity reduction by different gel plug removal agents. (**b**) Reaction rates of different agents with the polymer. (Error bars represent standard deviation from three measurements of the same sample.).

The reaction rates of the most effective inorganic oxidants were compared under the same conditions (Figure 1b). With sodium hypochlorite, sodium perborate, hydrogen peroxide, or potassium ferrate, at least 10 min was required for the viscosity to fall below 100 mPa·s. Sodium persulfate reduced the viscosity to below 100 mPa·s within 5 min. Among the five inorganic oxidants tested, sodium persulfate therefore provided the fastest reaction under these conditions and was selected based on its combined viscosity-reduction efficiency and reaction rate profile.

Dissolved persulfate is strongly oxidizing but nearly inert at low temperature without a catalyst. Its reaction rate with polymers is governed primarily by the persulfate concentration, temperature, and pH. Polymer-viscosity tests were therefore conducted at different temperatures, sodium persulfate concentrations, and pH values (Figure 2).

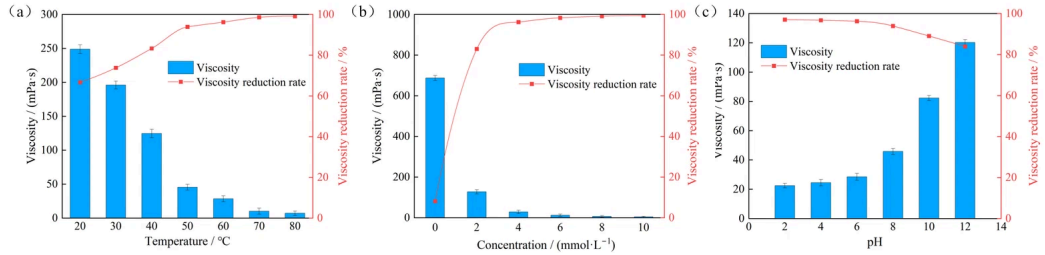


Figure 2. Effects of (**a**) temperature, (**b**) sodium persulfate concentration, and (**c**) pH on polymer-viscosity reduction. (Error bars represent standard deviation from three measurements of the same sample.).

Sodium persulfate showed little activity at low temperature, but the viscosity-reduction ratio increased with temperature and became substantial at 50 °C (Figure 2a). Heating promoted persulfate decomposition and increased the concentration of $SO_4^{\bullet-}$, the principal species responsible for viscosity reduction. At 65 °C, the viscosity-reduction ratio increased with sodium persulfate concentration and exceeded 90% at 4 mmol/L (Figure 2b). At 65 °C and 4 mmol/L of sodium persulfate, the reduction exceeded 95% at pH ≤ 6 but declined progressively under alkaline conditions as pH increased (Figure 2c).

Thus, polymer-viscosity reduction was positively associated with persulfate concentration and temperature and negatively associated with pH. For the target reservoir conditions in J Oilfield (65 °C and pH ≤ 6), 4 mmol/L of sodium persulfate was selected for subsequent experiments.

(2) Activator screening and concentration selection

Fe^{2+} activates sodium persulfate and promotes $SO_4^{\bullet-}$ generation, thereby enhancing polymer depolymerization. As the Fe^{2+} concentration increased, the viscosity of the treated polymer solution decreased, and the viscosity-reduction ratio rose from 96% to 99% (Figure 3a). Above 0.2 mmol/L of Fe^{2+}, both values reached a plateau. EPR measurements showed that the $SO_4^{\bullet-}$ concentration increased slowly at low Fe^{2+} concentrations, rose rapidly above 0.15 mmol/L, and reached a maximum at 0.25 mmol/L (Figure 3b). Accordingly, 0.25 mmol/L of Fe^{2+} was selected at 65 °C, pH 6, and 4 mmol/L of sodium persulfate.

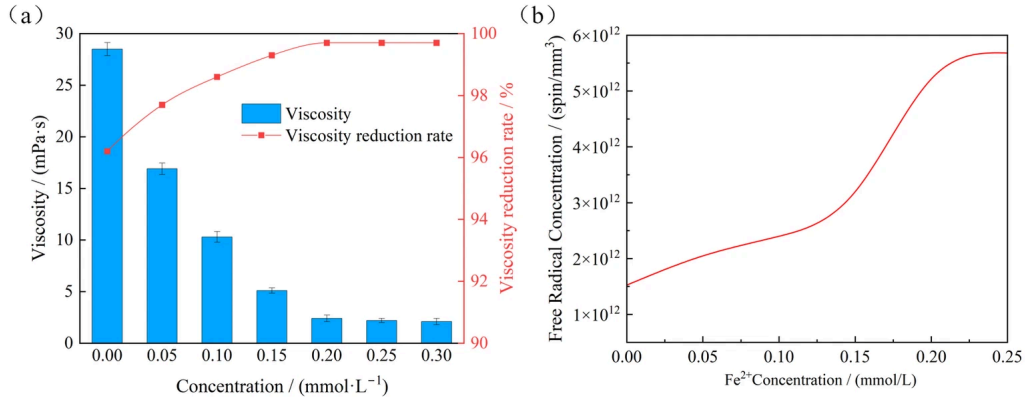


Figure 3. Effect of Fe^{2+} concentration on (**a**) polymer viscosity and (**b**) $SO_4^{\bullet -}$ concentration. (Error bars represent standard deviation from three measurements of the same sample.).

(3) Acid screening

Hydrochloric, hydrofluoric, and organic acids can dissolve polymer-associated formation deposits and the inorganic cores of polymer aggregates, thereby releasing entanglements among polymers, oil, and particulates. Sodium persulfate also reduced polymer viscosity more effectively under acidic conditions. Under alkaline conditions, metal ions in formation water can combine with OH^- to form precipitates and aggravate plugging. Acidic conditions are therefore more favorable for gel plug removal by the persulfate-based composite plugging removal agent.

To evaluate the corrosive effects of common acids on reservoir minerals and injection-production tubulars, SiO_2 and $CaCO_3$ specimens and N80 steel coupons were immersed in different 10 wt% acid solutions (Figure 4).

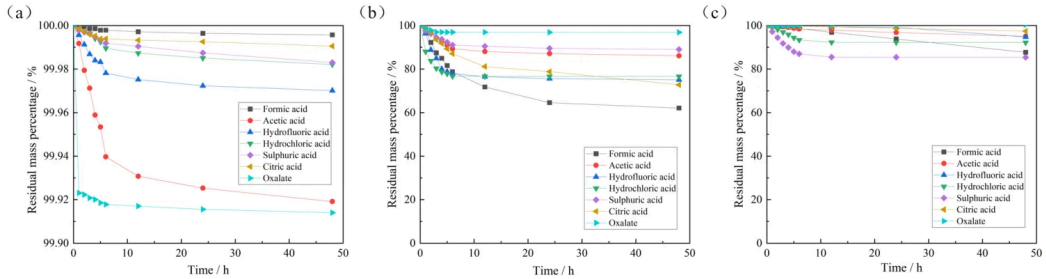


Figure 4. Effects of common acids on (**a**) SiO_2, (**b**) $CaCO_3$, and (**c**) N80 steel coupons.

All tested organic and inorganic acids caused less than 0.1% mass loss from SiO_2 after 48 h (Figure 4a). Formic and citric acids caused the least loss (<0.01%), followed by sulfuric, hydrochloric, and hydrofluoric acids (0.02–0.03%) and acetic and oxalic acids (0.07–0.09%). The order of increasing attack on SiO_2 was formic acid < citric acid < sulfuric acid < hydrochloric acid < hydrofluoric acid < acetic acid < oxalic acid.

For $CaCO_3$, oxalic acid caused the lowest 48 h mass loss (<5%), sulfuric and acetic acids caused losses of 10–20%, hydrofluoric, hydrochloric, and citric acids caused losses of 20–30%, and formic acid caused a loss of 40% (Figure 4b). The order of increasing attack was oxalic acid < sulfuric acid < acetic acid < hydrochloric acid < hydrofluoric acid < citric acid < formic acid.

Citric and acetic acids caused the least mass loss from N80 steel coupons (<5% after 48 h), followed by hydrofluoric and hydrochloric acids (5–10%) and formic and sulfuric acids (10–15%) (Figure 4c). Oxalic acid produced an apparent mass gain because a green flocculent layer adsorbed on the coupon surface. The order of increasing attack was ox-

alic acid (mass gain) < citric acid < acetic acid < hydrofluoric acid < hydrochloric acid < formic acid < sulfuric acid. Only single-acid corrosion screening tests were performed in this work to select an acid component with relatively low corrosivity. Corrosion performance of the full composite plug removal formulation under reservoir conditions has not been evaluated.

Carbonate minerals constitute the principal inorganic component of typical reservoir deposits, whereas the rock framework is dominated by SiO_2, and the tubulars are primarily made of N80 steel. Citric acid was therefore selected because it caused little damage to SiO_2 and N80 steel but effectively dissolved $CaCO_3$. Its field concentration should be selected for site-specific conditions and deposit composition.

(4) Oil-washing-agent screening

Field plugging deposits formed during polymer injection commonly contain polymers, inorganic particles, and crude oil. The influence of crude oil on depolymerization was therefore evaluated at 65 °C using polymer–oil mixtures of different compositions. The initial viscosities of the polymer and crude oil were 1236 and 700 mPa·s, respectively (Figure 5). As the oil fraction increased, the post-treatment viscosity increased and the viscosity-reduction ratio decreased. The polymer alone showed a reduction of 97.85%, and the reduction remained above 90% at 10% oil. Above 10% oil, performance deteriorated markedly, reaching only 41.51% at 40% oil. Crude oil therefore inhibited depolymerization. An oil-washing agent was required to emulsify the oil and separate it from the polymer, thereby improving contact between the persulfate and the polymer.

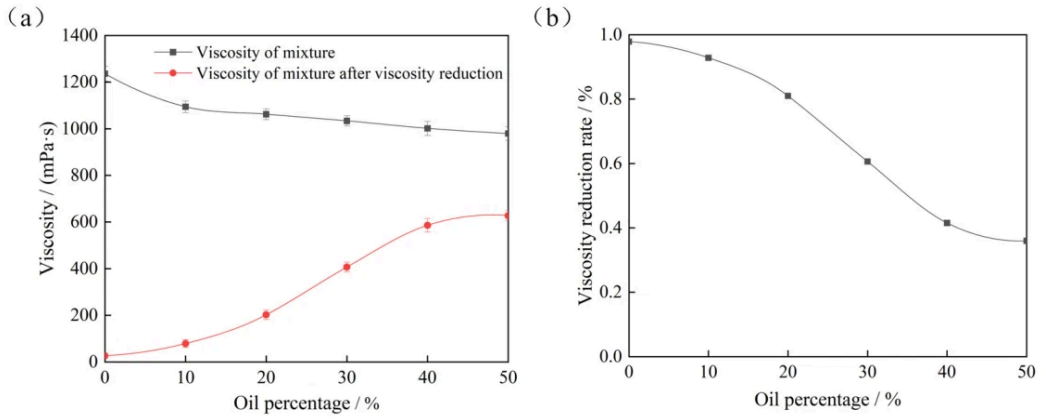


Figure 5. Effect of crude oil content on (**a**) mixture viscosity and (**b**) viscosity-reduction ratio. (Error bars represent standard deviation from three measurements of the same sample.).

Oil removal from contaminated sand was evaluated with different washing agents (Figure 6). Span 80 removed the largest oil volume (1.4 mL). CTAB, sodium secondary alkyl sulfonate, and OP-10 each removed 1.2 mL, whereas all other agents removed less than 1 mL. It should be noted that the separated upper oil volume is only a semi-quantitative indicator of oil-washing performance. Surfactant-induced emulsification may affect the volume of the separated oil phase and lead to deviation in quantitative evaluation. Span 80 shows relatively good oil removal performance under this test condition. Span 80 was therefore selected, with its field concentration to be selected for site conditions and deposit composition.

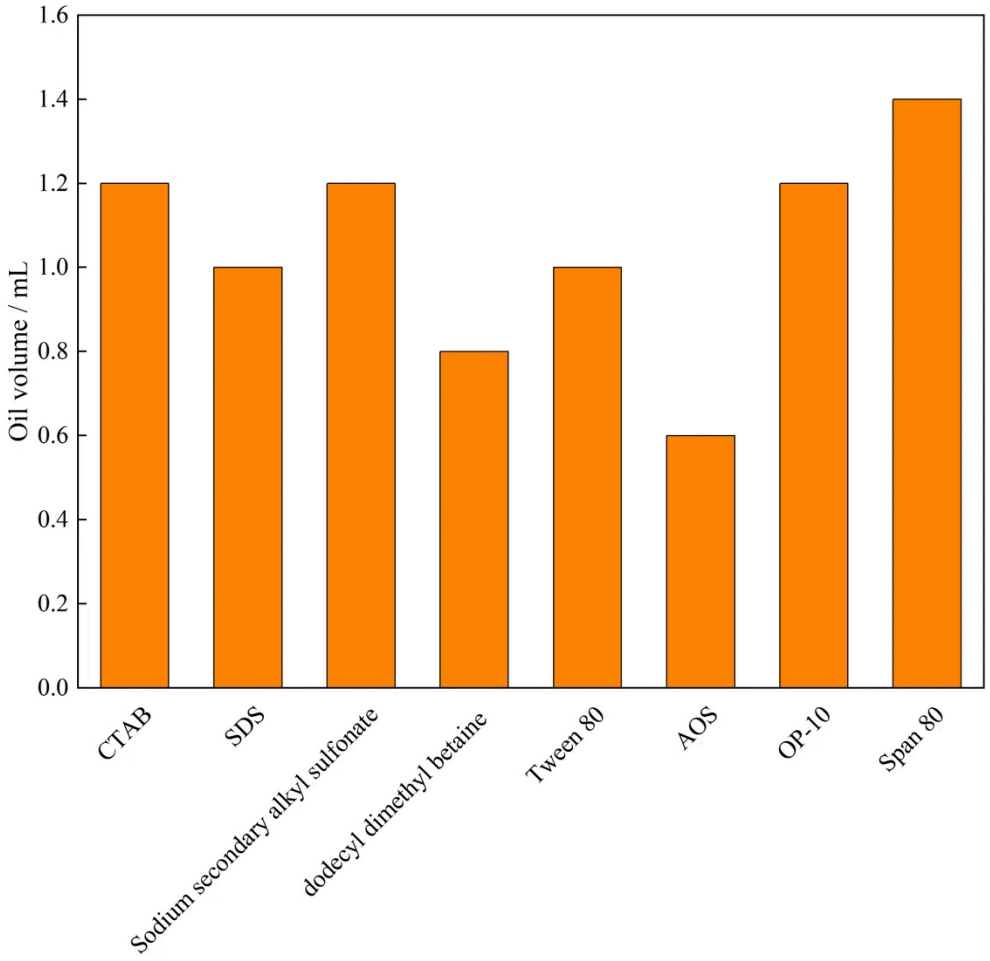


Figure 6. Oil removal from contaminated sand by different washing agents.

The final persulfate-based composite plugging removal agent for the experiment comprised 4 mmol/L of $Na_2S_2O_8$, 0.25 mmol/L of $FeSO_4$, 2 wt% citric acid, and 0.2 wt% Span 80. The concentrations of citric acid and Span 80 should be adjusted to the field conditions and deposit composition.

2.1.2. Static Characteristic of the Persulfate-Based Composite Plugging Removal Agent

Zeta-potential and optical-stability tests were conducted to assess the persulfate-based composite plugging removal agent stability (Figures 7 and 8). The zeta potential was −36.7 mV. Transmitted light intensity showed no appreciable change with time, indicating that the system remained stably dispersed at 65 °C and a salinity of 6864 mg/L.

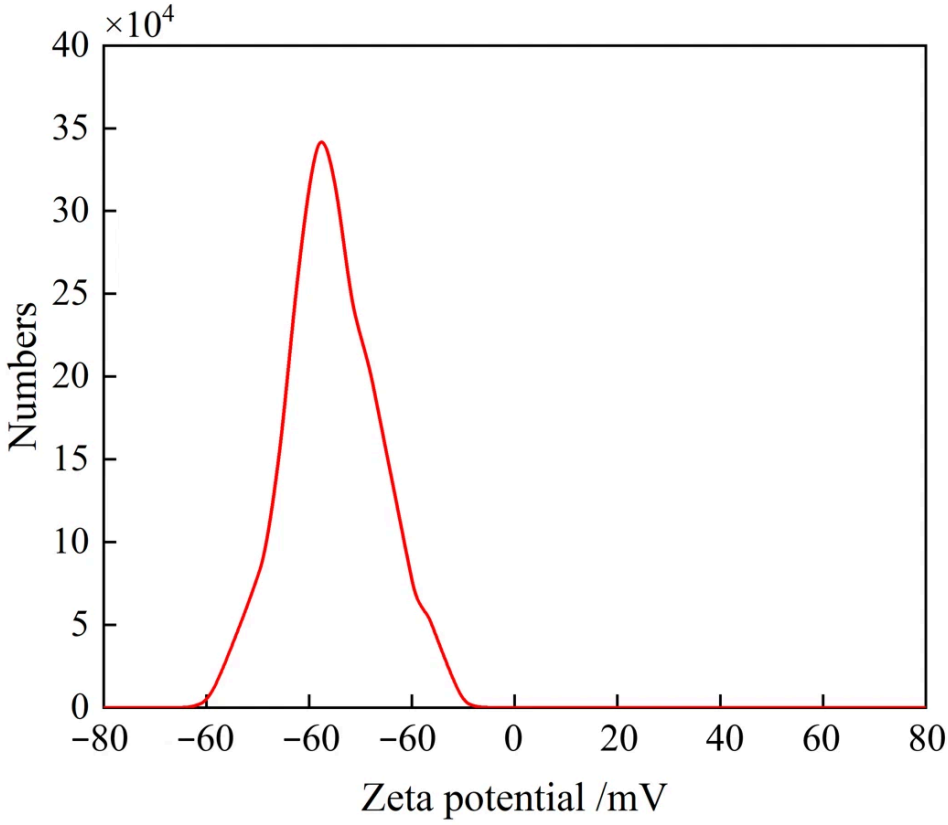


Figure 7. Zeta potential of the persulfate-based composite plugging removal agent.

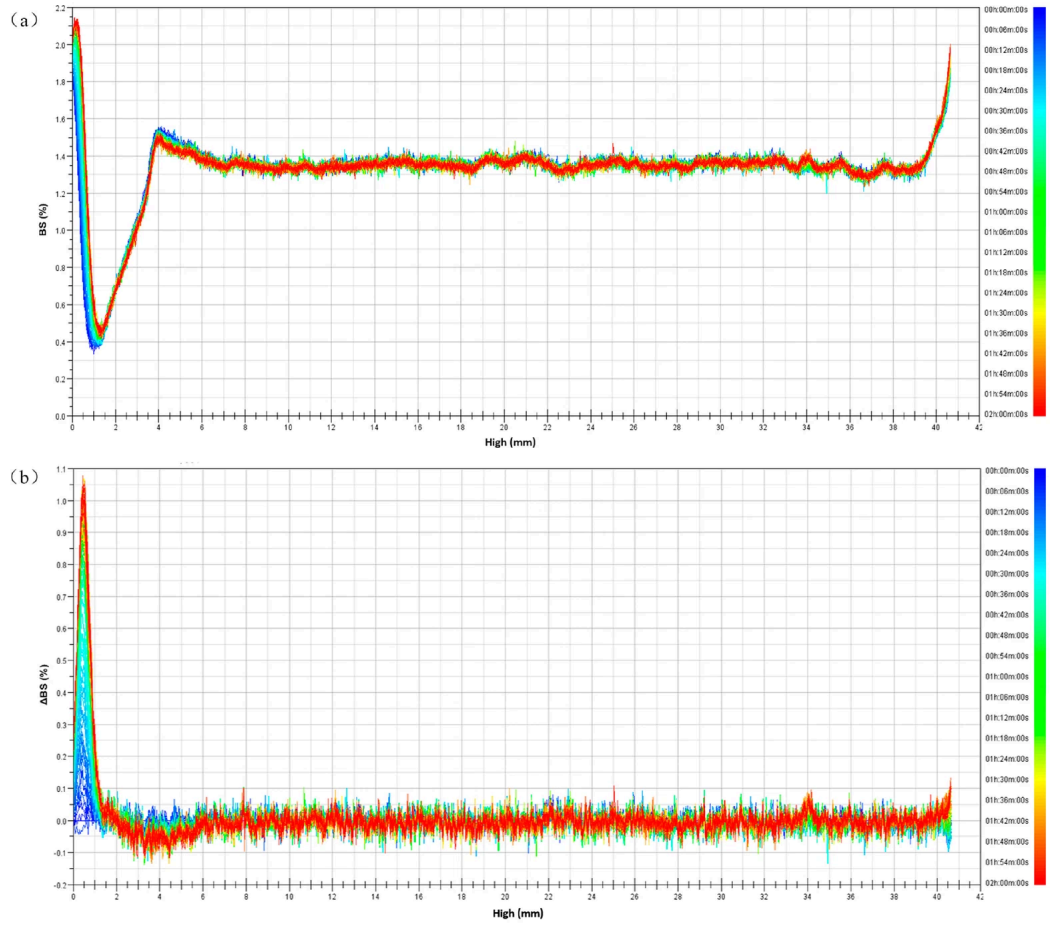


Figure 8. (a,b) Absorbance profile of the persulfate-based composite plugging removal agent over

time.

Polymers with relative molecular masses of 8.0×10^6 to 2.5×10^7 were prepared at 0.1 wt%. At 65 °C and a salinity of 6864 mg/L, each polymer solution was mixed with the persulfate-based composite plugging removal agent at a 1:1 mass ratio (Figure 9a). The different initial viscosities were obtained by preparing polyacrylamide solutions with different molecular weights. The initial viscosity increased with polymer molecular mass. After treatment, all viscosities decreased to below 50 mPa·s, corresponding to reductions greater than 95%.

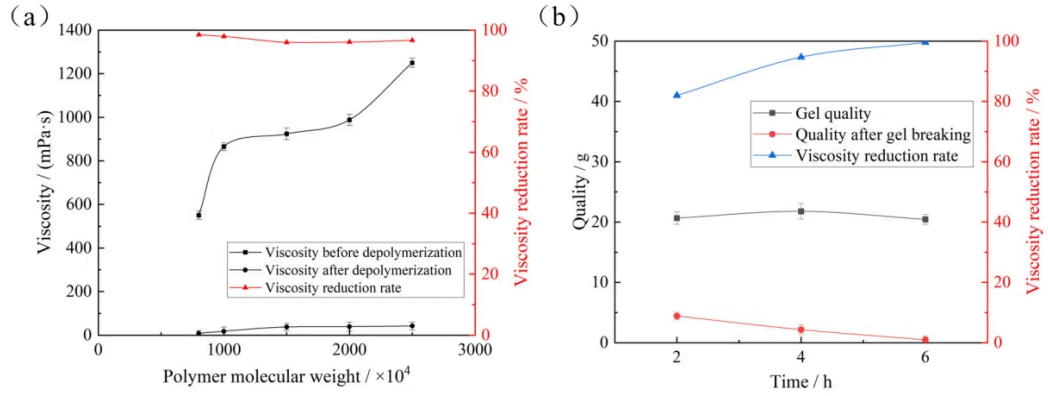


Figure 9. (**a**) Viscosity reduction of polymers with different molecular masses. (**b**) Gel removal performance of the persulfate-based composite plugging removal agent. (Error bars represent standard deviation from three measurements of the same sample.).

Gels prepared form polymers with a relative molecular mass of 2.5×10^7 were also treated with the persulfate-based composite plugging removal agent (Figure 9b). At 65 °C, the degradation ratio approached 95% after 4 h, and the gel was almost completely broken down after 6 h.

2.2. Depolymerization Mechanism of the Persulfate-Based Composite Plugging Removal Agent

2.2.1. Free-Radical Oxidation Mechanism

Sodium persulfate dissociates in water to form $S_2O_8^{2-}$ and Na^+. Heat and Fe^{2+} activate $S_2O_8^{2-}$ to generate $SO_4^{\bullet-}$, part of which reacts in water to form HO•. The published literature has proved that both radicals initiate chain oxidation of the polymer and generate polymer-centered radicals (P•). Subsequently, α- and β-scission cleaves C-C, C-H, and C-N bonds and is accompanied by decarboxylation (Figure 10). These chain reactions break intra- and intermolecular linkages, convert long polymer chains into shorter chains, disrupt the polymer network, and reduce solution viscosity [20,23,25]. The proposed reactions are given below.

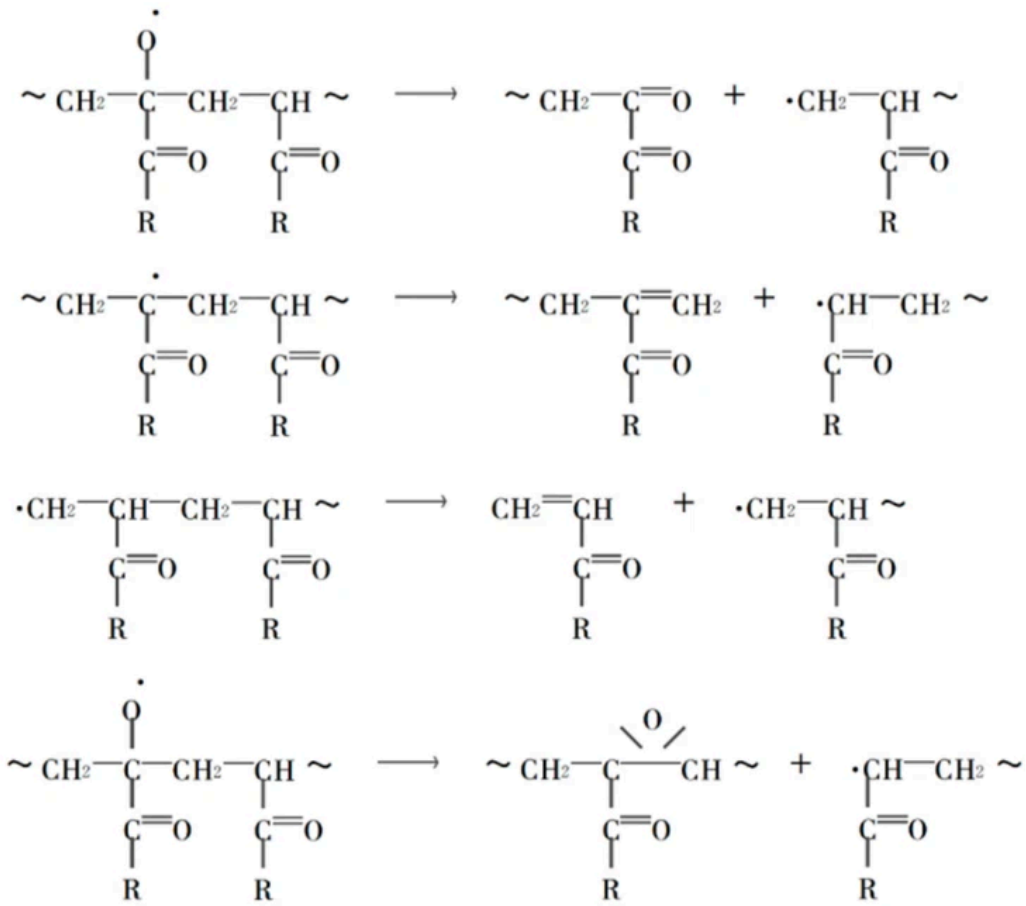


Figure 10. Proposed α- and β-scission pathways.

Thermal activation:

$$S_2O_8{}^{2-} \xrightarrow{heat} 2SO_4\cdot^{-} \quad (1)$$

Fe^{2+} activation:

$$Fe^{2+} + S_2O_8{}^{2-} \rightarrow Fe^{3+} + SO_4{}^{2-} + SO_4\cdot^{-} \quad (2)$$

Generation of polymer-centered radicals by $SO_4\bullet^{-}$:

$$SO_4\cdot^{-} + PH \rightarrow SO_4{}^{2-} + P\cdot + H^{+} \quad (3)$$

The α- and β-scission pathways are shown in Figure 10.

$SO_4\bullet^{-}$ and HO• are the principal reactive species responsible for polymer oxidation and viscosity reduction. Their identities and concentrations during depolymerization were examined by EPR. At 65 °C, pH 7, and 4 mmol/L of sodium persulfate, characteristic signals of both $SO_4\bullet^{-}$ and HO• were detected, indicating that both radicals participated in the chain oxidation reaction (Figure 11a).

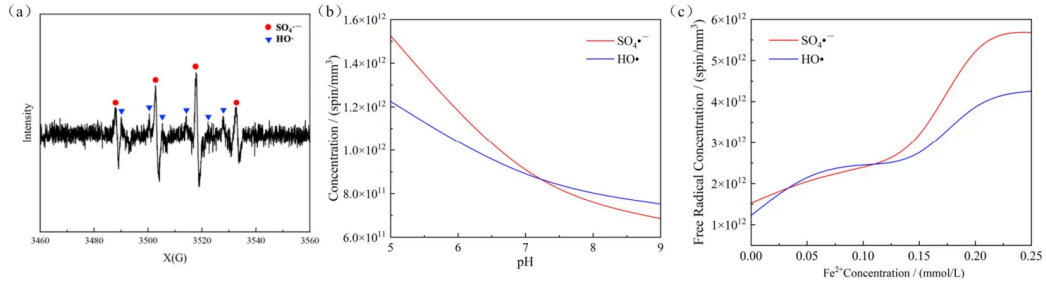


Figure 11. (**a**) EPR spectra of radicals generated by the persulfate-based composite plugging removal agent at pH 7. Radical concentrations as functions of (**b**) pH and (**c**) Fe^{2+} concentration.

SO_4•$^-$ can react in water to form HO•, which may subsequently generate O_2 through oxidation reactions and create a potential field safety hazard. By contrast, persulfate is relatively inert at low temperature without a catalyst, allowing the reaction rate and conditions to be controlled. Limiting the conversion of SO_4•$^-$ to HO• may therefore reduce the potential for O_2 generation. EPR measurements at different pH values showed that SO_4•$^-$ exceeded HO• below pH 7, and the difference increased as pH decreased (Figure 11b). Their concentrations were similar between pH 7 and 8, whereas HO• predominated above pH 8. This trend is consistent with conversion of SO_4•$^-$ to HO• through reaction with OH^- under alkaline conditions. Acidic conditions therefore favored SO_4•$^-$-dominated oxidation and more stable depolymerization performance.

Fe^{2+} promotes the conversion of $S_2O_8^{2-}$ to SO_4•$^-$ and thereby accelerates polymer oxidation. At 65 °C, pH 6, and 4 mmol/L of sodium persulfate, SO_4•$^-$ and HO• concentrations were similar below 0.15 mmol/L of Fe^{2+}, and both increased with Fe^{2+} concentration (Figure 11c). Above 0.15 mmol/L, SO_4•$^-$ exceeded HO•, and the difference increased. Both concentrations plateaued above 0.25 mmol/L, where their separation was greatest. An Fe^{2+} concentration of 0.25 mmol/L was therefore selected to favor SO_4•$^-$ generation. Radical scavenging experiments were not implemented in the present work, and we will design appropriate radical scavenging experiments in our subsequent investigation to quantify the contribution of each radical species.

2.2.2. Microscopic Depolymerization Mechanism

Figure 12 compares the particle-size distributions of the persulfate-based composite plugging removal agent and a 0.2 wt% polymer solution (relative molecular mass, 2.5×10^7) before and after treatment. Before treatment, polymer aggregates were mainly 500–2000 nm (Figure 12a). Hydrogen bonding, van der Waals forces, and other intermolecular interactions caused nanoscale polymer molecules to entangle into micrometer-scale aggregates. The persulfate-based composite plugging removal agent itself showed populations at 200–1000 and 4000–7000 nm, attributable to surfactant micelles in the concentrated formulation (Figure 12b). After treatment, the main particle-size range decreased to 10–30 nm, with a minor population at 200–500 nm (Figure 12c). This change indicates disintegration of large entangled polymer aggregates, which may originate from both covalent main chain cleavage and disassembly of physical intermolecular entanglements. This viewpoint has also been validated by previous related studies [23,25].

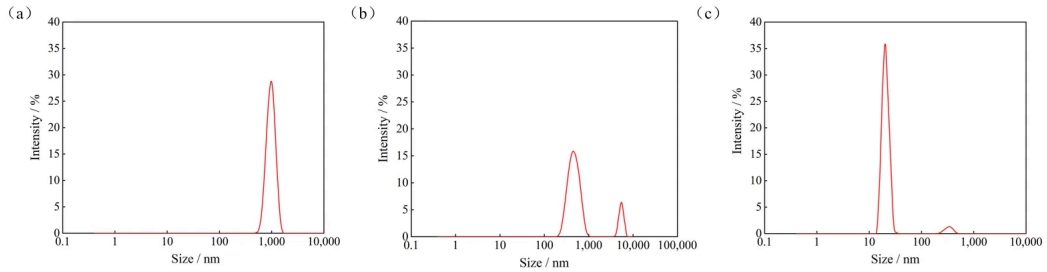


Figure 12. Particle-size distributions of (**a**) the untreated polymer solution, (**b**) the persulfate-based composite plugging removal agent, and (**c**) the polymer solution after treatment.

Changes in polymer microstructure were examined by SEM (Figure 13). Before treatment, the polymer formed a dense, entangled three-dimensional network that increased aqueous-phase viscosity. After persulfate-based composite plugging removal agent addition, many intermolecular connections were broken, the dense network collapsed, and loosely connected small aggregates formed. The remaining connections were thin and susceptible to further cleavage. Fragmentation of long carbon chains also disrupted the polymer backbone, maybe accounting for the observed viscosity reduction. The above conclusions regarding polymer morphological changes and viscosity reduction induced by carbon chain scission are inferred from the conclusions of the published literature and experimentally observed phenomena. It should be noted that SEM observation is performed on freeze-dried samples. Freeze-drying processing may change native polymer morphology to some extent. Therefore, SEM images serve for comparative qualitative analysis of network change before and after degradation, rather than representing in situ native gel morphology under reservoir aqueous conditions.

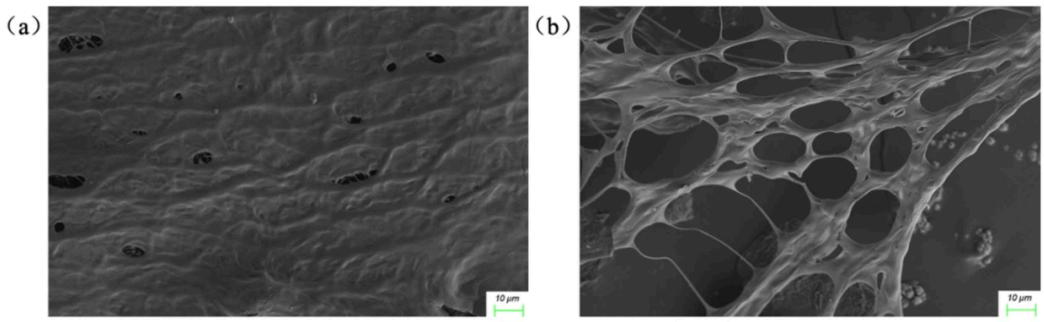


Figure 13. SEM images of the polymer solution (**a**) before and (**b**) after persulfate-based composite plugging removal agent injection.

2.3. Core Plugging After Polymer Flooding and Dynamic Removal Performance

2.3.1. Plugging and Removal Rules After Long-Term Polymer Injection

Ten long-term polymer-injection experiments were conducted using cores with an initial permeability of approximately 500 mD (Figures 14 and 15). Polymer injection markedly reduced permeability, and subsequent water injection did not restore it. Thus, water flooding alone could not readily remove polymers retained in the porous medium. As the injected polymer volume increased, adsorption and retention increased, permeability declined, and the residual resistance factor rose from approximately 2.8 after 1 PV to approximately 6.5 after 10 PV. SEM images of sectioned cores showed abundant retained polymers in the pores. The adsorbed polymer chains were entangled into a three-dimensional network that obstructed pore space and reduced permeability.

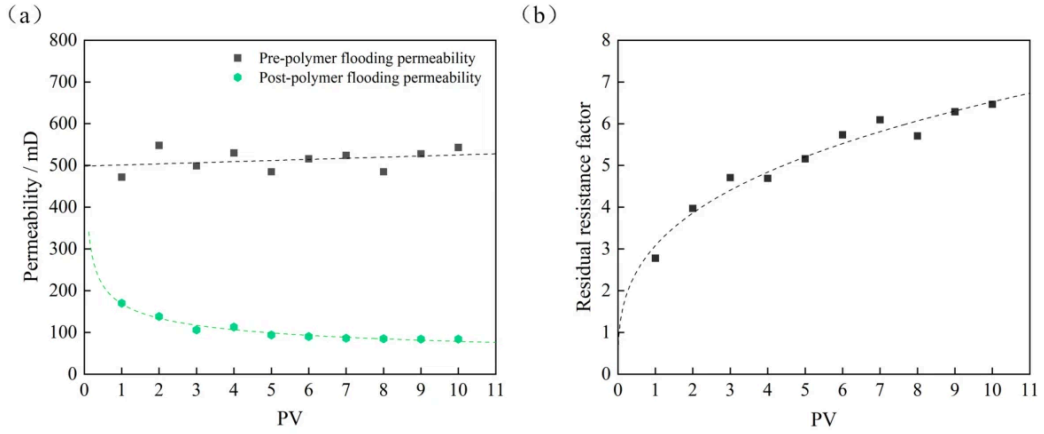


Figure 14. Changes in (**a**) core permeability and (**b**) residual resistance factor after polymer flooding.

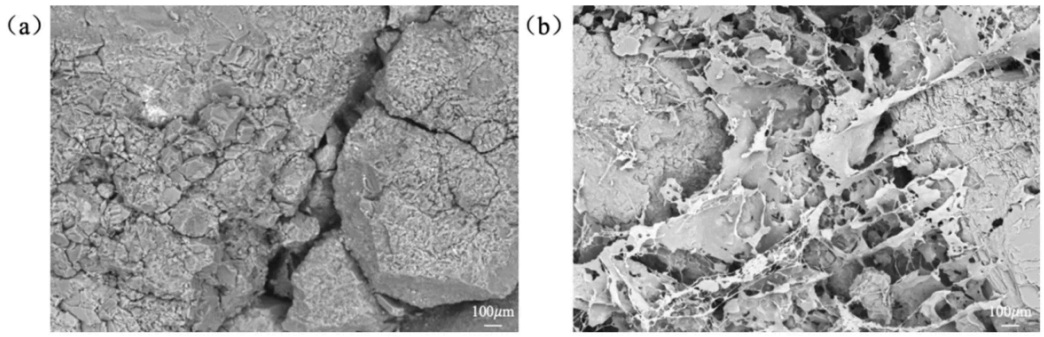


Figure 15. SEM images of core samples (**a**) before and (**b**) after polymer injection.

The persulfate-based composite plugging removal agent was then injected into the polymer-flooded cores (Figure 16). Polymer injection had reduced permeability below 200 mD in every core. After treatment, permeability recovered to above 400 mD, corresponding to more than 80% recovery, while the residual resistance factor decreased to 1.0–1.5. These results show that the persulfate-based composite plugging removal agent effectively removed polymer-related plugging from the porous medium.

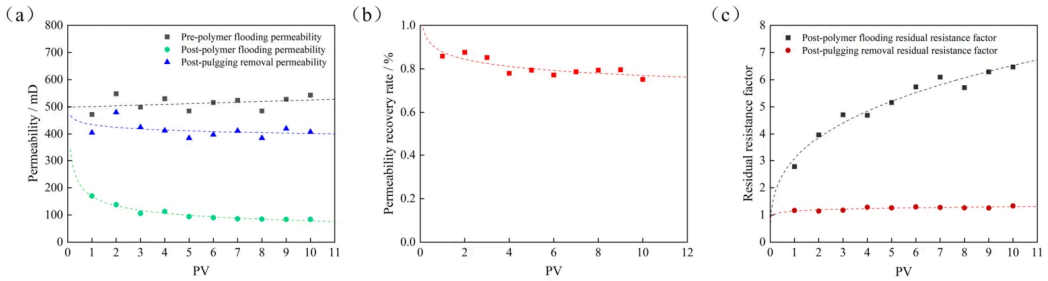


Figure 16. Core properties before and after plugging removal: (**a**) permeability, (**b**) permeability recovery, and (**c**) residual resistance factor.

2.3.2. Dynamic Plugging Removal Performance in Long Cores

In the polymer injection control, injection pressure increased continuously and reached 1189 kPa after 1 PV of the polymer had been injected (Figure 17a). The produced-fluid viscosity reached 1496 mPa·s, indicating polymer breakthrough and saturation of the core (Figure 17b). After switching to water, pressure continued to rise and produced-fluid viscosity remained near 1450 mPa·s. When the cumulative injected vol-

ume reached 1.6 PV, pressure and produced-fluid viscosity decreased sharply, possibly because the water formed a preferential flow channel. Pressure subsequently stabilized near 200 kPa, and viscosity fell below 200 mPa·s and continued to decrease with water injection.

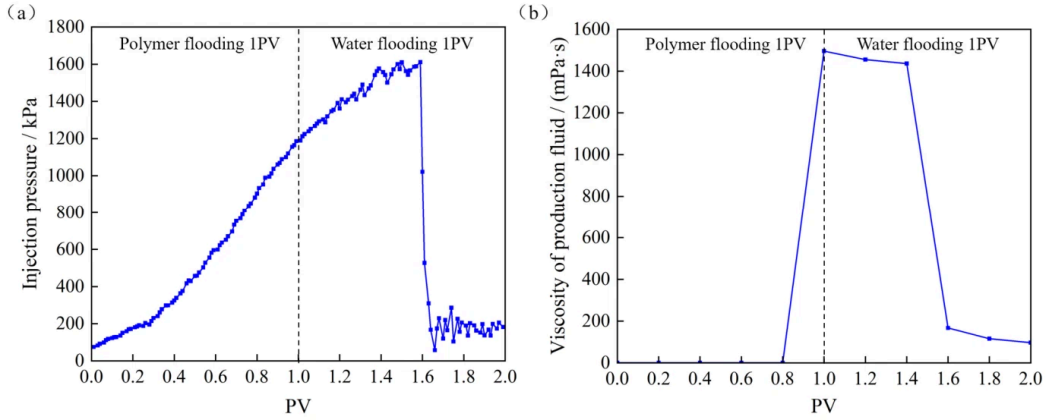


Figure 17. Polymer injection experiment in a long core: (**a**) injection pressure and (**b**) produced-fluid viscosity.

In the removal experiment, injection pressure and produced-fluid viscosity reached 1281 kPa and 1496 mPa·s, respectively, after 1 PV of the polymer was injected (Figure 18). Injection of 0.1 PV of the persulfate-based composite plugging removal agent followed by shut-in substantially lowered the restart pressure, and a further 0.2 PV of the persulfate-based composite plugging removal agent caused a continued decline. After the treatment was displaced with water, both pressure and produced-fluid viscosity fell sharply. Following 0.5 PV of water, viscosity was below 100 mPa·s and pressure stabilized near 100 kPa. The persulfate-based composite plugging removal agent therefore reduced the viscosity of the adsorbed and retained polymer in the core, relieved plugging, and improved injectivity. Independent replicate coreflooding experiments were not performed in this work, and the coreflooding results provide a qualitative trend reference.

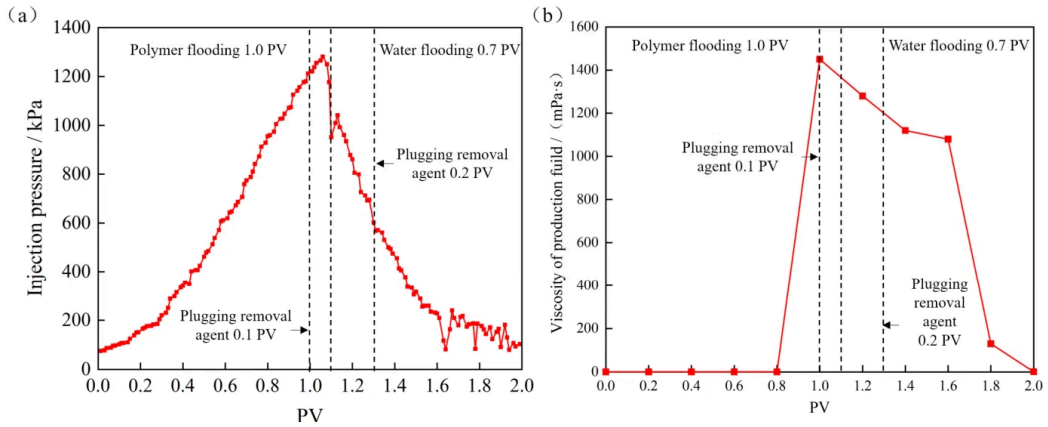


Figure 18. Plugging removal experiment in a long core: (**a**) injection pressure and (**b**) produced-fluid viscosity.

High-permeability cores (2000 mD) were selected to avoid excessive pressure drop and equipment overpressure risk during long-term polymer injection displacement. These experiments focus on obtaining the qualitative variation laws of polymer-induced plugging and plug removal. The experimental trends can provide guidance for the target

field reservoir (100–500 mD), whereas the quantitative results from these high-permeability cores cannot be directly extrapolated to field conditions.

2.4. Pilot Test of Persulfate-Based Composite Plugging Removal Agent

2.4.1. Reservoir Background of J Oilfield

The reservoir is composed mainly of fine silty sandstone containing 50–60% quartz and 30–35% feldspar. The cement is argillaceous (15%), with almost no carbonate. Primary intergranular pores dominate the storage space. Porosity is high, generally 27–31%, whereas permeability is moderate at 100–500 mD. The permeability variation coefficient is 0.75, indicating strong heterogeneity. The reservoir contains heavy crude oil with a low pour point, a density of 0.94 g/cm^3, and a viscosity of 78–89 mPa·s at 50 °C. Well D exhibited obvious near-wellbore plugging after long-term polymer injection, and the compositional analysis of the sampled plugging materials is shown in Table 1. Although the reservoir rock matrix contains negligible carbonate minerals, carbonate precipitates formed by formation water scaling are present in near-wellbore plugging deposits.

Table 1. Composition of the near-wellbore plugging.

No.	Component	Content (wt.%)
1	Water	59.3
2	Polymer flocculent material	12.4
3	Clay and mechanical impurities	7.4
4	Carbonates (Ca and Mg)	6.6
5	Bacteria and their metabolites	4.9
6	Analytical loss	3.4
7	Basic iron carbonate	3.1
8	Oil sludge	1.6
9	Iron sulfide	1.3
	Total	100.0

2.4.2. Gel Plug Removal Pilot Test

(1) Well characteristics

Well D was initially produced for fluid withdrawal and was scheduled for conversion to injection after six months. The perforated interval comprised three zones (I, II, and III) with a total effective thickness of 19.5 m and a mid-reservoir depth of 1699.3 m. The maximum well deviation was 38.94°. Each zone had an independent premium-screen sand-control completion.

(2) Injection performance and operational problem

Before treatment, Well D used a downhole string for simultaneous measurement and adjustment, with independent injection into Zones I, II, and III. Injection pressure was 12.5 MPa, casing pressure was 0 MPa, actual injection was 345 m^3/d, and the allocated injection rate was 340 m^3/d under high-pressure conditions. A zonal allocation test showed that Zone III could not meet its target rate.

(3) Injection design of persulfate-based composite plugging removal agent

Zone III was treated separately, whereas Zones I and II were treated commingled. The persulfate-based composite plugging removal agent targeted the gel plug, and acid targeted inorganic deposits. Zones I and II received 15 m^3 of the persulfate-based composite plugging removal agent plus 20 m^3 of acid, and Zone III received 20 m^3 of the per-

sulfate-based composite plugging removal agent plus 20 m^3 of acid.

The field plug removal treatment fluid was prepared on site with the following concentrations: 4 mmol/L of $Na_2S_2O_8$, 0.25 mmol/L of $FeSO_4$, 2 wt% citric acid, and 0.2 wt% Span 80. The subsequent acid stimulation treatment adopted 10 wt% citric acid.

(4) Gel plug removal performance

During forward injection of the persulfate-based composite plugging removal agent, injection pressure gradually decreased from 16.5 to approximately 16 MPa, while the pumping rate increased from 0.8 to 0.9 m^3/min. After a 24 h shut-in, the rate increased further to approximately 1.0 m^3/min at 16.5 MPa, indicating that the injected fluid had entered the formation and improved injectivity.

During the subsequent acid injection, injection pressure decreased from 16.5 to approximately 14 MPa and the pumping rate increased from 1.0 to 1.1 m^3/min, indicating removal of near-wellbore damage. After acid injection, wellhead pressure fell from approximately 14 MPa to 0.26 MPa within 5 min during pressure falloff. The operation was completed on 5 May 2021. Relative to pretreatment values, injection pressure decreased from 12.5 to 5.5 MPa and the daily injection rate increased from 340 to 360 m^3/d. The apparent injectivity index increased from 27.2 to 65.5 m^3/(d·MPa), or 2.4-fold, confirming substantial remediation of near-wellbore damage.

The field case shows improved injection performance after sequential treatment with the plugging removal agent and subsequent acid stimulation. Since the two treatments were carried out successively in one well, their individual contributions cannot be quantitatively separated. Therefore, this field result reflects the overall effect of the combined remediation strategy for polymer plugging. Long-term monitoring data are unavailable due to the data confidentiality restrictions of the field operator, so the sustained effectiveness of the treatment cannot be evaluated in this work.

3. Conclusions

An efficient persulfate-based composite plugging removal agent was developed for a polymer-flooded reservoir in J Oilfield. Its viscosity-reduction performance, reaction mechanism, core-scale plugging removal efficiency, and field applicability were systematically evaluated. The system removed gel-related plugging from porous media and restored permeability, providing a practical option for improving reservoir performance after polymer flooding.

(1) The persulfate-based composite plugging removal agent comprised 4 mmol/L of $Na_2S_2O_8$, 0.25 mmol/L of $FeSO_4$, 2 wt% citric acid, and 0.2 wt% Span 80. At 65 °C and a salinity of 6864 mg/L, it remained stably dispersed (zeta potential, −36.7 mV) and reduced the viscosity of polymers with different molecular masses by more than 95%.

(2) The microscopic degradation mechanism was elucidated based on the published literature and experimental results. Fe^{2+} activation generated $SO_4^{\bullet-}$ and HO•. At pH ≤ 6, $SO_4^{\bullet-}$ dominated the controlled radical reaction. Chain oxidation and disruption caused the fracture of the three-dimensional polymer network and reduced aggregate size from 500–2000 nm to 10–30 nm. Acidic conditions maintained a higher $SO_4^{\bullet-}$ concentration and stable depolymerization performance. The Fe^{2+}-activated system showed low activity at low temperature but effective viscosity reduction at elevated temperature.

(3) The residual resistance factor increased with injected polymer PV, confirming progressively severe core plugging. Persulfate-based composite plugging removal agent treatment reduced the residual resistance factor from 6.5 to 1.0–1.5 and restored more than 80% of the initial permeability.

(4) The J Oilfield trial demonstrates improved injection performance after sequential plug removal and acid stimulation treatments. The injection pressure reduced from 12.5

to 5.5 MPa, and the apparent injectivity index increased by 2.4 times, demonstrating effective remediation of near-wellbore damage after polymer flooding.

4. Materials and Methods

4.1. Materials and Equipment

The polymer used in this study is partially hydrolyzed polyacrylamide (HPAM, Shanghai Meryer Biochemical Technology Co., Ltd./Shanghai Macklin Biochemical Co., Ltd, Shanghai, China). The hydrolysis degree ranges from 25% to 30%; the molecular mass ranges from 8.0×10^6 to 2.5×10^7; the solid content is ≥ 88%. All acids and other common reagents were of analytical grade and were purchased from Shanghai Meryer Biochemical Technology Co., Ltd. and Shanghai Macklin Biochemical Co., Ltd. The crude oil and formation water were sampled from J Oilfield. The formation water salinity of J Oilfield is shown in Table 2. The experimental equipment used in this study is listed in Table 3.

Table 2. Formation water salinity of J Oilfield.

Oilfield	Ion Content of Formation Water/(mg·L^{-1})							Total Salinity/(mg·L^{-1})
	$Na^+ + K^+$	Mg^{2+}	Ca^{2+}	Cl^-	SO_4^{2-}	HCO_3^-	CO_3^{2-}	
J Oilfield	2229	12	40	1684	346	2355	198	6864

Table 3. Experimental equipment.

Instrument	Model	Manufacturer
Analytical balance	BSA423S	Sartorius,Göttingen, Germany
Rotational viscometer	DV-II+ Pro	Brookfield, Middleboro, MA, USA
Constant-temperature oven	HW-II	Haian Petroleum Scientific Research Equipment, Nantong, China
Precision pH meter	pH-100B	Lichen Instrument Technology, Shaoxing, China
Rheometer	Physica MCR 301	Anton Paar, Graz, Austria
Particle-size and zeta-potential analyzer	Nano-ZS2000	Malvern Panalytical, Malvern, UK
Multiple light-scattering analyzer	Turbiscan Lab Expert	Formulaction, Toulouse, France
EPR spectrometer	Bruker EMXPlus-10	Bruker, Billerica, MA, USA
Vacuum freeze dryer	FD-B10N-50	Shengwei Electronic Technology, Shanghai, China
Field-emission SEM	Quanta 200F	FEI, Hillsboro, OR, USA

4.2. Experimental Methods

4.2.1. Static Evaluation Experimental Methods

(1) Viscosity testing experiment

The required mixed solutions were prepared according to the experimental design. Their viscosities were measured with an Anton Paar rheometer and a rotational viscometer. The rotational speed was set to 10 rpm (corresponding shear rate of 1.7 s^{-1}). Before recording data, samples were equilibrated at the target experimental temperature (65 °C) for 10 min to achieve thermal equilibrium. Each sample was measured in triplicate, and

the average value was reported.

(2) Scanning electron microscopy (SEM) experiment

Aliquots of the prepared solutions were freeze-dried. Their microstructures were then imaged with a field-emission scanning electron microscope.

(3) Zeta-potential and particle-size testing experiment

Dynamic light-scattering (DLS) measurements for particle-size distribution and zeta-potential were performed using a Malvern Nano-ZS2000 analyzer. Before measurement, polymer-containing samples were diluted with simulated formation water (salinity 6000 mg/L) at a dilution ratio of 1:100 (*v*/*v*) to avoid multiple-scattering effects. The refractive index was set to 1.47 for polymer aggregates and 1.33 for the aqueous dispersion medium. For every sample, three independent replicate measurements were conducted at a constant temperature of 65 °C. The polydispersity index (PDI) was recorded automatically by the instrument software. For multimodal particle-size distributions, the built-in non-negative least squares (NNLS) algorithm was applied to resolve individual particle-size populations. The intensity-weighted particle-size distribution was adopted for result interpretation.

(4) Electron paramagnetic resonance spectroscopy testing experiment

A 4 mmol/L aqueous sodium persulfate ($Na_2S_2O_8$) solution was prepared at 65 °C, and $FeSO_4$ was added at the specified concentration. The radical species and concentrations generated during the reaction were measured with a Bruker EMXPlus-10 electron paramagnetic resonance (EPR) spectrometer.

The spin trapping agent DMPO (5,5 dimethyl 1 pyrroline N oxide) was applied for radical capture. EPR acquisition parameters: microwave power = 20 mW; modulation amplitude = 1.0 G; sweep width = 100 G; receiver gain = 1×10^5. Radical concentration was semi-quantitatively calculated by double integrating the characteristic EPR signal peaks, calibrated against a standard TEMPO sample. Each test was repeated three times. The uncertainty mainly originates from the short lifetime of radical adducts, side reactions during the trapping process, and baseline deviation during integration.

(5) Activator testing experiment

A 0.2 wt% polymer solution and a 4 mmol/L sodium persulfate solution were prepared, together with $FeSO_4$ solutions at the specified concentrations. The polymer and sodium persulfate solutions were mixed, and a predetermined amount of $FeSO_4$ solution was added. After thorough mixing, viscosity was measured with a rotational viscometer, and the viscosity-reduction ratio was calculated using Equation (1).

(6) Acid testing experiment

Solutions of different acids were prepared at 10 wt%. Pre-weighed $CaCO_3$ or SiO_2 rock specimens and N80 steel coupons were immersed in the acid solutions and reacted in an oven at 60 °C. At 1 h intervals, the specimens were removed, dried at 60 °C, weighed, and returned to their original solutions. The experiment was terminated after 48 h.

(7) Oil-washing-agent testing experiment

Formation core from J Oilfield was crushed and sieved to obtain sand grains of uniform size. The grains were mixed with polymer and J Oilfield crude oil, aged at 65 °C for 7 d, and freeze-dried under vacuum for 12 h. Surfactant solutions were prepared at 0.2 wt%. Oil-contaminated sand (3 g) and surfactant solution (10 mL) were mixed in a test tube and heated at 65 °C for 1 h, after which the volume of oil in the upper part of the tube was recorded.

(8) Compositional analysis of the sampled plugging materials

Near-wellbore plugging deposit samples were collected from the wellbore of Well D during workover operation. Three parallel samples were taken for compositional analy-

sis. Water content was determined by gravimetric method after drying at 105 °C for 24 h. Organic components (polymer and crude oil) were extracted and quantified by solvent extraction and gravimetric separation. Inorganic mineral components were analyzed by X-ray diffraction (XRD, Bruker, Billerica, MA, USA) and chemical titration. The relative standard deviation of each component measurement is less than 5%.

4.2.2. Depolymerization and Plugging Removal Tests

(1) Polymer depolymerization

The polymer was mixed separately with water and with the persulfate-based composite plugging removal agent and reacted in a constant-temperature water bath at 65 °C for 4 h. The viscosity of each mixture was then measured with a rotational viscometer, and the viscosity-reduction ratio was calculated using Equation (4):

$$\eta_1 = \frac{\mu_1 - \mu_2}{\mu_1} \times 100\,\% \quad (4)$$

where η1 is the viscosity-reduction ratio (%),μ_1 is the initial viscosity of the polymer solution (mPa·s), and μ_2 is the viscosity after the degradation reaction (mPa·s).

(2) Gel plug removal

The polymer was mixed with the persulfate-based composite plugging removal agent and reacted in a constant-temperature water bath for a specified period. The residue was collected on a filter screen, and the degradation ratio was calculated using Equation (5):

$$\eta_2 = \frac{m_p + m_w - m_a}{m_p} \times 100\,\% \quad (5)$$

where η_2 is the polymer degradation ratio (%), m_p is the initial gel mass (g), m_w is the filter-screen mass (g), and m_a is the combined mass of the post-reaction residue and filter screen (g).

4.2.3. Coreflooding and Dynamic Plugging Removal Tests

Coreflooding experiments were carried out at 65 °C using simulated formation water. The core confining pressure was 10 MPa, and backpressure was 5 MPa. The polymer injection rate was 0.2 mL/min, while the injection rate of the water and plug removal agent was set to 0.5 mL/min. The differential pressure across the core was automatically recorded every 10 s, and the core is water-wet, consistent with the target reservoir.

(1) Long-term polymer injection tests

The core properties are listed in Table 4. After water and oil saturation, the cores were aged at 65 °C for 7 d. Different pore volumes (PVs) of polymer solution were then injected according to the experimental design. Water injection followed the polymer slug, and the post-polymer-flooding permeability and pressure were recorded. Next, 0.1 PV of the persulfate-based composite plugging removal agent was injected. The cores were shut in for 1 h and then flooded with water, after which permeability and pressure were measured again. The residual resistance factor was defined as the ratio of permeability before polymer flooding to that after polymer flooding. Permeability recovery was defined as the ratio of permeability after persulfate-based composite plugging removal agent injection to that before polymer flooding.

Table 4. Core properties for long-term polymer injection tests.

No.	Core Type	Diameter (cm)	Length (cm)	Pore Volume (mL)	Porosity (%)	Permeability (mD)
1	Natural core	2.5	10	14	28.54	472
2	Natural core	2.5	10	15	30.57	548
3	Natural core	2.5	10	16	32.61	499
4	Natural core	2.5	10	17	34.65	530
5	Natural core	2.5	10	15	30.57	485
6	Natural core	2.5	10	16	32.70	516
7	Natural core	2.5	10	15	30.51	524
8	Natural core	2.5	10	14	29.86	485
9	Natural core	2.5	10	15	31.42	528
10	Natural core	2.5	10	15	30.82	543

(2) Dynamic plugging removal tests of cores after polymer flooding

Two parallel experiments were conducted: a polymer injection control and a persulfate-based composite plugging removal agent injection test. A total of two long cores was used for the plugging removal tests, and the individual core properties are listed in Table 5. Core L-1 was used for polymer injection and the plugging test, and Core L-2 was adopted for the plugging removal test. A polymer solution with a concentration of 0.1 wt% and a viscosity of 1280 mPa·s was used in this experiment. After saturation with water and oil, the cores were aged at 65 °C for 7 d before testing. The initial water saturation and initial oil saturation were calculated based on the injection volumes recorded during the core saturation process.

Table 5. Long-core properties for the plugging removal tests.

No.	Core Type	Diameter (cm)	Length (cm)	Pore Volume (mL)	Porosity (%)	Permeability (mD)
L-1	Natural core	4.5	4.5	21	29.60	1999
L-2	Natural core	4.5	4.5	22	30.93	2000

At 65 °C, 1 PV of polymer solution was injected to saturate the core, followed by 1 PV of water. Pressure was recorded throughout the experiment, and the produced fluid was collected for viscosity measurement with a rotational viscometer. Then, 1 PV of polymer solution was injected to saturate the core, followed by 0.1 PV of the persulfate-based composite plugging removal agent. The inlet and outlet were closed for 1 h. A further 0.2 PV of the persulfate-based composite plugging removal agent was then injected, followed by another 1 h shut-in and 0.7 PV of water. Pressure was recorded throughout, and the viscosity of the produced fluid was measured with a rotational viscometer. The schematic diagram of the coreflooding experiments is shown in Figure 19.

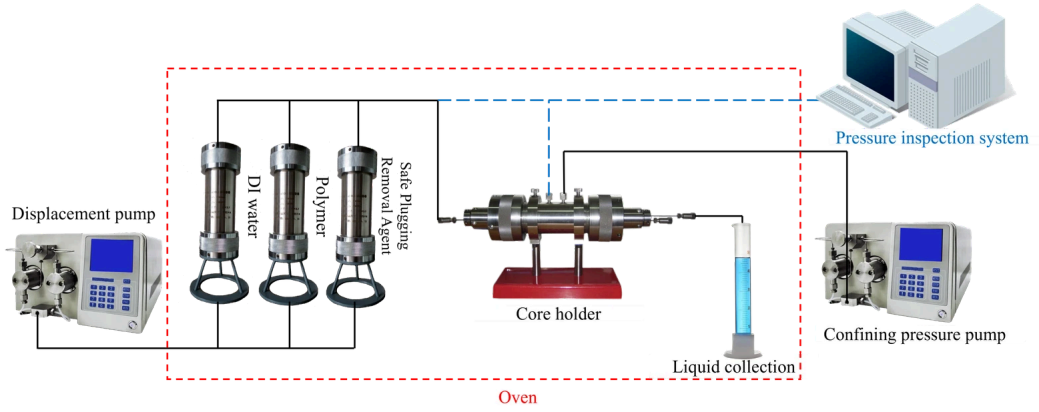


Figure 19. Schematic diagram of coreflooding experiments.

Author Contributions: Conceptualization, Y.W. and J.H.; methodology, Y.W. and J.W.; validation, Y.P.; formal analysis, Y.W., Y.P., Y.L. and N.L.; investigation, Y.L. and R.M.; data curation, Y.W., Y.P., Y.L. and R.M.; writing—original draft preparation, Y.W.; writing—review and editing, Y.W., J.W., N.L. and J.H.; visualization, N.L.; project administration, J.W., R.M. and J.H.; funding acquisition, J.W. All authors have read and agreed to the published version of the manuscript.

Funding: China National Petroleum Corporation Science and Technology Project (Grant No.2026ZYGJCS002 and No.2026ZYGJCS006).

Institutional Review Board Statement: Not applicable.

Informed Consent Statement: Not applicable.

Data Availability Statement: Data are available from the corresponding author upon reasonable request.

Acknowledgments: The authors gratefully acknowledge the financial support of the China National Petroleum Corporation Science and Technology Project (Grant No.2026ZYGJCS002 and No.2026ZYGJCS006).

Conflicts of Interest: The authors declare that this study received funding from China National Petroleum Corporation (CNPC). The funder was involved in the study design.

References

1. Wever, D.; Picchioni, F.; Broekhuis, A. Polymers for enhanced oil recovery: A paradigm for structure–property relationship in aqueous solution. *Prog. Polym. Sci.* **2011**, *36*, 1558–1628. [Google Scholar] [CrossRef]
2. Kamal, M.S.; Sultan, A.S.; Al-Mubaiyedh, U.A.; Hussein, I.A. Review on Polymer Flooding: Rheology, Adsorption, Stability, and Field Applications of Various Polymer Systems. *Polym. Rev.* **2015**, *55*, 491–530. [Google Scholar] [CrossRef]
3. Sheng, J.J.; Leonhardt, B.; Azri, N. Status of Polymer-Flooding Technology. *J. Can. Pet. Technol.* **2015**, *54*, 116–126. [Google Scholar] [CrossRef]
4. Saboorian-Jooybari, H.; Dejam, M.; Chen, Z. Heavy oil polymer flooding from laboratory core floods to pilot tests and field applications: Half-century studies. *J. Pet. Sci. Eng.* **2016**, *142*, 85–100. [Google Scholar] [CrossRef]
5. Wang, D.; Dong, H.; Lv, C.; Fu, X.; Nie, J. Review of Practical Experience by Polymer Flooding at Daqing. *SPE Reserv. Eval. Eng.* **2009**, *12*, 470–476. [Google Scholar] [CrossRef]
6. Standnes, D.C.; Skjevrak, I. Literature review of implemented polymer field projects. *J. Pet. Sci. Eng.* **2014**, *122*, 761–775. [Google Scholar] [CrossRef]
7. Seright, R.S.; Wang, D. Polymer flooding: Current status and future directions. *Pet. Sci.* **2023**, *20*, 910–921. [Google Scholar] [CrossRef]

8. Seright, R.S.; Campbell, A.R.; Mozley, P.S.; Han, P. Stability of partially hydrolyzed polyacrylamides at elevated temperatures in the absence of divalent cations. *SPE J.* **2010**, *15*, 341–348. [Google Scholar] [CrossRef]
9. Shupe, R.D. Chemical Stability of Polyacrylamide Polymers. *J. Pet. Technol.* **1981**, *33*, 1513–1529. [Google Scholar] [CrossRef]
10. Ma, Q.; Shuler, P.J.; Aften, C.W.; Tang, Y. Theoretical studies of hydrolysis and stability of polyacrylamide polymers. *Polym. Degrad. Stab.* **2015**, *121*, 69–77. [Google Scholar] [CrossRef]
11. Sugar, A.; Serag, M.; Buttner, U.; Fahs, M.; Habuchi, S.; Hoteit, H. Experimental and numerical investigation of polymer pore-clogging in micromodels. *Sci. Rep.* **2023**, *13*, 8245. [Google Scholar] [CrossRef] [PubMed]
12. Bessaies-Bey, H.; Fusier, J.; Harrisson, S.; Destarac, M.; Jouenne, S.; Passade-Boupat, N.; Lequeux, F.; de Lacaillerie, J.-B.D.; Sanson, N. Impact of polyacrylamide adsorption on flow through porous siliceous materials: State of the art, discussion and industrial concern. *J. Colloid Interface Sci.* **2018**, *531*, 693–704. [Google Scholar] [CrossRef] [PubMed]
13. Hao, T.; Zhong, L.; Liu, J.; Sun, H.; Zhu, T.; Zhang, H.; Wu, S. Mechanistic Study on the Decrease in Injectivity during Salt-Resistant Polymer Flooding. *ACS Omega* **2022**, *7*, 11293–11304. [Google Scholar] [CrossRef] [PubMed]
14. Li, Y.; Fu, M.; Hou, B.; Zhang, Z.; Sun, R. Experimental Study on Blockage Mechanism and Blockage Locations for Polymer-Flooded Reservoirs in the Henan Oilfield. *Geofluids* **2021**, *2021*, 6669921. [Google Scholar] [CrossRef]
15. Al-Hajri, S.; Mahmood, S.M.; Abdulrahman, A.; Abdulelah, H.; Akbari, S.; Saraih, N. An Experimental Study on Hydrodynamic Retention of Low and High Molecular Weight Sulfonated Polyacrylamide Polymer. *Polymers* **2019**, *11*, 1453. [Google Scholar] [CrossRef] [PubMed]
16. Seright, R.S.; Seheult, J.M.; Talashek, T. Injectivity Characteristics of EOR Polymers. In Proceedings of the SPE Annual Technical Conference and Exhibition, Denver, CO, USA, 21–24 September 2008. [Google Scholar]
17. Wang, Z.; Jiang, J.; Ni, H.; Huang, W.; Geng, L.; Cao, M.; Peng, H. Study on the Morphological Distribution and Formation Mechanisms of Residual Polymer in Polymer-Containing Wastewater. *ACS Omega* **2026**, *11*, 15283–15292. [Google Scholar] [CrossRef] [PubMed]
18. Gao, J.; Lu, X.; He, X.; Liu, J.; Zheng, K.; Cao, W.; Cui, T.; Sun, H. Effect Evaluation and Action Mechanism Analysis of "Profile Control + Plugging Removal" after Chemical Flooding. *Gels* **2022**, *8*, 396. [Google Scholar] [CrossRef] [PubMed]
19. Xiong, B.; Loss, R.D.; Shields, D.; Pawlik, T.; Hochreiter, R.; Zydney, A.L.; Kumar, M. Polyacrylamide degradation and its implications in environmental systems. *npj Clean Water* **2018**, *1*, 17. [Google Scholar] [CrossRef]
20. House, D.A. Kinetics and Mechanism of Oxidations by Peroxydisulfate. *Chem. Rev.* **1962**, *62*, 185–203. [Google Scholar] [CrossRef]
21. Neta, P.; Huie, R.E.; Ross, A.B. Rate constants for reactions of inorganic radicals in aqueous solution. *J. Phys. Chem. Ref. Data* **1988**, *17*, 1027–1289. [Google Scholar] [CrossRef]
22. Anipsitakis, G.P.; Dionysiou, D.D. Radical Generation by the Interaction of Transition Metals with Common Oxidants. *Environ. Sci. Technol.* **2004**, *38*, 3705–3712. [Google Scholar] [CrossRef] [PubMed]
23. Wacławek, S.; Lutze, H.V.; Grübel, K.; Padil, V.V.T.; Černík, M.; Dionysiou, D.D. Chemistry of persulfates in water and wastewater treatment: A review. *Chem. Eng. J.* **2017**, *330*, 44–62. [Google Scholar] [CrossRef]
24. Pu, J.Y.; Li, G.S.; Song, X.Z.; Luo, S.H.; Wang, B. Fabrication of Thermal-controlled Ammonium Persulfate Nanocapsules and Degradation of Insoluble Residue in Slickwater. *J. Oilfield Chem.* **2024**, *41*, 627–634. [Google Scholar]
25. Huang, S.; Guo, X.; Duan, W.; Cheng, X.; Zhang, X.; Li, Z. Degradation of high molecular weight polyacrylamide by alkali-activated persulfate: Reactivity and potential application in filter cake removal before cementing. *J. Pet. Sci. Eng.* **2019**, *174*, 70–79. [Google Scholar] [CrossRef]
26. Huang, S.; Li, Z.; Chen, C.; Tang, S.; Cheng, X.; Guo, X. Synergetic activation of persulfate by heat and Fe(II)-complexes for hydrolyzed polyacrylamide degradation at high pH condition: Kinetics, mechanism, and application potential for filter cake removal during cementing in CO_2 storage wells. *Sci. Total Environ.* **2020**, *713*, 136561. [Google Scholar] [CrossRef] [PubMed]
27. Sun, M.; Qiao, M.X.; Wang, J.; Zhai, L.F. Free-radical induced chain degradation of high-molecular-weight polyacrylamide in a heterogeneous electro-Fenton system. *ACS Sustain. Chem. Eng.* **2017**, *5*, 7832–7839. [Google Scholar] [CrossRef]
28. Qi, C.M.; Xia, Y.; Tang, S.F.; Zhao, L.J. Acid-Oxygen Synergistic Technology for Targeted Dissolution of Hybrid Organic–Inorganic Blockages in Low-Permeability Reservoirs. *ACS Omega* **2025**, *10*, 49721–49731. [Google Scholar] [CrossRef] [PubMed]

Disclaimer/Publisher's Note: The statements, opinions and data contained in all publications are solely those of the individual author(s) and contributor(s) and not of MDPI and/or the editor(s). MDPI and/or the editor(s) disclaim responsibility for any injury to people or property resulting from any ideas, methods, instructions or products referred to in the content.